THE JOURNAL OF PHYSICAL CHEMISTRY C

Article

pubs.acs.org/JPCC

How Density Functional Theory Surface Energies May Explain the Morphology of Particles, Nanosheets, and Conversion Films Based on Layered Double Hydroxides

Tiago L. P. Galvão,*[,†] Cristina S. Neves,[†] Mikhail L. Zheludkevich,[†,‡] José R. B. Gomes,[§] João Tedim,*[,†] and Mário G. S. Ferreira[†]

[†]CICECO-Aveiro Institute of Materials, Department of Materials and Ceramic Engineering, University of Aveiro, 3810-193 Aveiro, Portugal

[‡]Institute of Materials Research, Helmholtz-Zentrum Geesthacht, Centre for Materials and Coastal Research GmbH, Max-Planck-Strasse 1, 21502 Geesthacht, Germany

[§]CICECO-Aveiro Institute of Materials, Department of Chemistry, University of Aveiro, 3810-193 Aveiro, Portugal

Supporting Information

ABSTRACT: Conversion films based on layered double hydroxides constitute an important and environmentally friendly technology for the corrosion protection of aeronautical structures. Unfortunately, the morphology of layered double hydroxide (LDH) conversion films is still not well understood. In the present work, the structure and driving forces behind the morphology of zinc−aluminum LDH conversion films on aluminum alloy 2024 (AA2024) are explained from the perspective of molecular modeling. Since LDH particles are the core structures of LDH conversion films, the first step in this work was to understand the relation between structure and morphology of the particles themselves and the single-layer nanosheets that constitute them. Results regarding LDH's crystallites, particles, and conversion films obtained using X-ray diffraction (XRD), dynamic light scattering (DLS), scanning electron microscopy (SEM), and atomic force microscopy (AFM) are interpreted using periodic model density functional theory (DFT) calculations. On the basis of the understanding of the formation of LDH particles and their exfoliation to obtain single-layer nanosheets, for the first time, LDH conversion films have been modeled using periodic model DFT. The results point to a preferential orientation of the cationic layers perpendicular to the surface, thus explaining the film morphology (SEM and AFM) and providing a rational for their crystallization process.

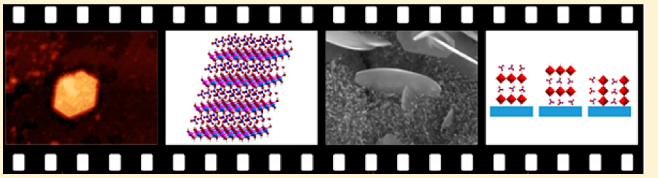

1. INTRODUCTION

In this work, we explore the structural features that are responsible for the morphology of conversion films based on layered double hydroxides (LDHs) grown on an aluminum substrate. LDH particles are basic building blocks of LDH conversion films.[1] Therefore, to understand the nanostructured films, it is necessary to understand the relation between structure and morphology of the particles themselves and the single-layer nanosheets that constitute them.

Understanding the formation of LDHs is fundamental to optimize their structure, size, and morphology for numerous applications such as catalysis,[2] batteries,[3] extraction,[4] or pharmaceuticals.[5] LDHs are also explored as additives for self-healing protective coatings[6] because of their ability to simultaneously release corrosion inhibitors[7] while absorbing corrosive anionic species.[8] As the need for large-scale production of LDHs increases, their synthetic process and formation mechanism as particles,[9−13] nanoclusters,[14] or nanoscrolls,[15] on surfaces[16] or into colloids,[17] also gains more interest.

First, we investigated the formation of LDH particles and their exfoliation[18−23] into single-layer nanosheets to increase the surface area.[19] The exfoliation of LDHs enhances their catalytic activity for oxygen evolution reaction (OER) involved in energy storage[18,23] and is useful to prepare LDHs for subsequent modification for biocompatible drug delivery.[24] Atomic force microscopy (AFM), X-ray diffraction (XRD),[25] and dynamic light scattering (DLS)[25] results were elucidated in terms of the energies of different exposed surfaces of LDH particles, obtained computationally using periodic model density functional theory (DFT) calculations. These conclusions were used to comprehend the molecular interactions ruling the growth pattern of LDH conversion films onto aluminum substrates.[1,26]

Generally, conversion films consist in a first coating layer grown directly on top of a metallic substrate to provide corrosion protection by barrier effect and to promote adhesion between the metal and the following layers of a coating system.[27] In a previous study, Tedim et al.[1] developed a methodology to grow in situ a nanostructured film of Zn−Al

Received: October 28, 2016
Revised: December 20, 2016
Published: December 28, 2016

DOI: 10.1021/acs.jpcc.6b10860
J. Phys. Chem. C XXXX, XXX, XXX−XXX

LDHs directly onto the surface of aluminum alloys, taking advantage of the dissolution of Al^{3+} from the surface.[26,28] The second two-valent cation (Zn^{2+}) is supplied from the treatment bath. This approach[1] makes possible to intercalate corrosion inhibitors by a subsequent step of ion-exchange providing the LDH conversion films with the same active protective functionality as LDH particles[7] but with the advantage of being near the metallic surface. LDH particles typically exhibit a platelike morphology.[25] When LDHs are grown directly onto aluminum alloys, these plates are assembled perpendicularly to the surface[1,26,29,30] as illustrated in Figure 1.

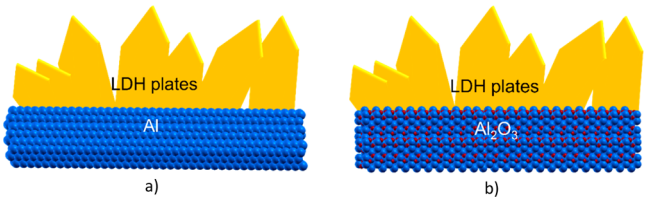

Figure 1. Illustration of the perpendicular assembling of LDH plates on the (a) bare aluminum and (b) aluminum oxide surfaces (sphere color code: Al, light blue; O, red). Figure not drawn to scale.

Herein, the formation and growth of LDH particles is investigated by means of AFM and scanning electron microscopy (SEM) complemented with additional information about the energies of different exposed surfaces from DFT calculations using periodic structural models of LDH clusters interacting with aluminum surfaces.

The material investigated in this work was zinc−aluminum LDH with a Zn:Al ratio of 2:1 and the nitrate anion intercalated (Zn(2)Al−NO_3), since it can be easily synthesized as individual particles[25] and as conversion films onto aluminum substrates.[1] It is also a functional material on its own.[8] Moreover, the nitrate anion can easily allow us to obtain single-layer nanosheets,[18−22] and it can also be easily substituted by other functional anions,[7] which makes it a precursor for many applications.[7,18−22] Our aim was to determine the direction of the LDH plates on the metallic surface in terms of morphology and structure. For the aluminum surfaces, two different periodic models were examined: Al(111) and hydroxylated aluminum terminated α-Al_2O_3(0001).

2. EXPERIMENTAL SECTION

Materials. $Zn(NO_3)_2{\cdot}6H_2O$ (99%), $Al(NO_3)_3{\cdot}9H_2O$ (98.5%), $NaNO_3$ (99.5%), NaOH (98%), and NH_4OH (25%) were obtained from Sigma-Aldrich and were used without any further purification.

Zn(2)Al−NO_3 Particles. The samples of LDH particles used in this work for AFM analysis were those synthesized in a previous work[25] by coprecipitation at constant pH followed by the growth of the crystals by hydrothermal treatment. During the coprecipitation step, a 50 mL mixture of 0.5 M $Zn(NO_3)_2{\cdot}6H_2O$ and 0.25 M $Al(NO_3)_3{\cdot}9H_2O$ solution was added dropwise to a 100 mL solution of 1.5 M $NaNO_3$ under vigorous stirring at room temperature. During this step, the pH was controlled using a pH meter and was kept nearly constant (±0.5) by simultaneous addition of 2 M NaOH (~50 mL). Afterward, the obtained product was subjected to hydrothermal treatment using different combinations of time and temperature, and finally, it was centrifuged and washed four times with boiled and nitrogen-saturated distilled water (decarbonated water).

Different combinations of coprecipitation pH and time and temperature of hydrothermal treatment were tested [(pH = 10, T = 325 K, t = 4 h), (pH = 10, T = 373 K, t = 2 h), (pH = 10, T = 373 K, t = 4h), and (pH = 8.5, T = 372 K, t = 4 h)] since they affect the LDH crystallite and particle sizes.[25] The obtained samples were used for AFM characterization.

Preparation of Aluminum Substrates. Aluminum alloy 2024 (AA2024) plates were rinsed successively with deionized water, followed by acetone for removal of particulates and degreasing. Then, AA2024 plates were surface treated using an industrial/commercial procedure. Briefly, the plates were immersed twice in a 2.5% Gardacid solution for 45 s followed by acid etching through immersion of the plates in Turco Liquid Smutgo NC for 7 min. Each step was followed by washing with deionized water. Finally, the AA2024 plates were dried in air.

Synthesis of Zn(2)Al−NO_3 LDH Conversion Films. Following a procedure described in previous studies,[1,26,29] the treated AA2024 plates were immersed in a $Zn(NO_3)_2$ solution (5 mM) under near neutral pH and a hydrothermal treatment of 373 K for 4 h. Subsequently, the plates were washed with ultrapure water and ethanol and were dried in air. The obtained samples were used for AFM and SEM characterization.

Characterization of Materials. The morphology of the LDH particles and conversion films was characterized by AFM and SEM.

The AFM was performed using a commercial AFM system (Veeco multimode with nanoscope III controller) under ambient conditions. The experiments were carried out with silicon cantilevers (NCH probes from Nanoworld) with a resonant frequency (f_0) of approximately 320 kHz and a nominal spring constant of 42 N m^{-1}. The samples of LDH particles were prepared by depositing 200 μL of LDH aqueous solution (50 mg L^{-1}) on poly-L-lysine coated glass slides and carefully dried before analysis. The samples of LDH conversion films were analyzed as obtained after the synthesis without any further treatment. Images were collected in tapping mode and were analyzed using the Gwyddion software (http://gwyddion.net/).

The SEM experiments were performed with a Hitachi S-4100 operating at an acceleration voltage of 25 kV.

3. COMPUTATIONAL SECTION

Periodic model DFT calculations were performed with the Quantum ESPRESSO (QE)[31] and the Perdew−Burke−Ernzerhof (PBE)[32] exchange-correlation functional. The computational approach followed in this study was successfully applied by other authors[33] and in a previous study from our research group[25] in the study of LDHs. The nuclei and core electrons were described by ultrasoft pseudopotentials[34] available for PBE in the QE Web site (http://www.quantum-espresso.org/pseudopotentials/). The Kohn−Sham orbitals were expanded using planewave basis sets with 40 Ry cutoff for kinetic energy and 240 Ry cutoff for charge density. The first Brillouin zone integrations were performed with the Marzari−Vanderbilt smearing method[35] using a smearing parameter of 0.02 and a 2 × 2 × 1 k-point mesh.[36] The optimization procedure was stopped after the forces acting on all atoms in a structure were lower than 10^{-2} Ry.

The periodic structure of Zn(2)Al−NO_3 was modeled by a $(\sqrt{3} \times \sqrt{3})R30°$ supercell, as described by other authors.[33,37]

DOI: 10.1021/acs.jpcc.6b10860
J. Phys. Chem. C XXXX, XXX, XXX−XXX

The $[Zn_2Al(OH)_6](NO_3)\cdot H_2O$ supercell (Figure 2) contains one $[Zn_2Al(OH)_6]^+$ cationic layer counterbalanced in the

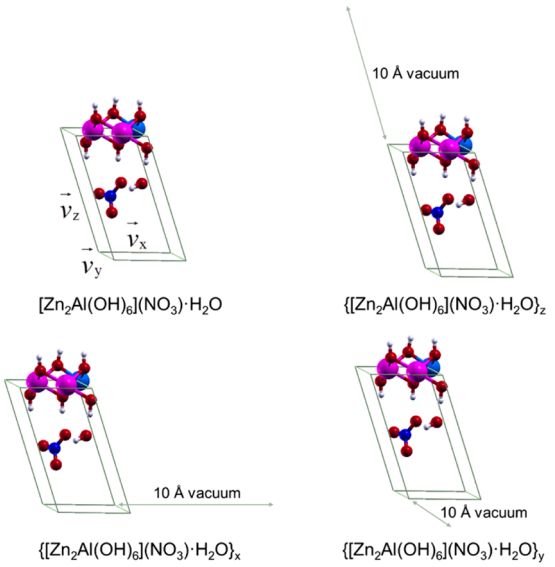

Figure 2. Representation of the $[Zn_2Al(OH)_6](NO_3)\cdot H_2O$, $\{[Zn_2Al(OH)_6](NO_3)\cdot H_2O\}_x$, $\{[Zn_2Al(OH)_6](NO_3)\cdot H_2O\}_y$ and $\{[Zn_2Al(OH)_6](NO_3)\cdot H_2O\}_z$ supercells (spheres color code: Zn, pink; Al, light blue; O, red; N, blue; H, white).

interlayer by one nitrate anion solvated with a single water molecule. The number of solvating water molecules was chosen according to thermogravimetric measurements performed in a previous study.[38]

The supercell corresponds to the *R*3*c* space group and is described by two lattice parameters, *a* and *c*, which define the lattice vectors $\vec{v}_x(2\sqrt{3}a, 0, 0)$, $\vec{v}_y(-\sqrt{3}a, 3a, 0)$, and $\vec{v}_z(a/2, \sqrt{3}a/2, c/3)$.[33,37] The size and ratio of metal cations in the LDH cationic layers define the lattice parameter *a*, which was calculated from the position of the (110) reflection, according to $a = 2\cdot d_{(110)}$, obtained in a previous work.[25] The interlayer distance occupied by the NO_3^- anion defines the *c* lattice parameter and was optimized in this work. The relative position of the NO_3^- anion to the cationic layers was examined in more detail in a previous work.[25]

To calculate the relative energies of different LDH exposed surfaces (E_x, E_y, and E_z) after their optimization, a vacuum region of 10 Å was defined for one of the three directions defined by each axis that characterizes the repetition of the supercell, according to Figure 2, while keeping the periodicity of the other two directions unaltered.

To better illustrate the energetic effects of forming LDH particles, the interaction energy between the respective edges of each surface was calculated taking the energy of the fully periodic $[Zn_2Al(OH)_6](NO_3)\cdot H_2O$ supercell and the energy of each surface $\{[Zn_2Al(OH)_6](NO_3)\cdot H_2O\}_x$, $\{[Zn_2Al(OH)_6](NO_3)\cdot H_2O\}_y$, and $\{[Zn_2Al(OH)_6](NO_3)\cdot H_2O\}_z$, according to eq 1.

$$\{[Zn_2Al(OH)_6](NO_3)\cdot H_2O\}_A \rightarrow [Zn_2Al(OH)_6](NO_3)\cdot H_2O \qquad A = x, y, \text{ or } z \tag{1}$$

The effect of substituting water in the interlayer of the LDH−NO_3 structure by formamide, which is known to favor the exfoliation of LDHs,[19] was investigated. The water molecule solvating the nitrate was replaced by a formamide molecule, and the $[Zn_2Al(OH)_6](NO_3)\cdot NH_2COH$ supercell was used for the optimization. The optimization of the structure was also performed for two and three solvent molecules of water and formamide per anion.

To understand the orientation of LDH plates on the surface of the metallic substrate, the interaction between one $[Zn_2Al(OH)_6](NO_3)\cdot H_2O$ cluster per supercell and two aluminum surfaces [Al(111) and hydroxylated aluminum terminated α-Al_2O_3(0001)] was analyzed. Three coordination modes were analyzed in this work, as represented in Figure 3:

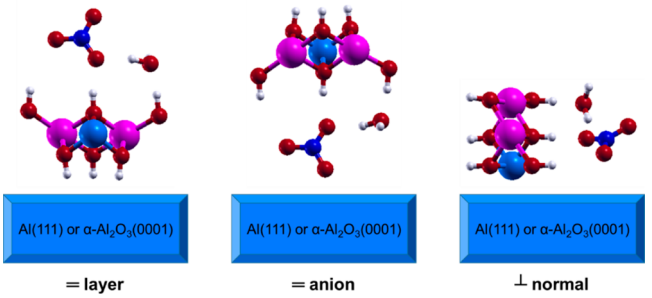

Figure 3. Types of interaction between one $[Zn_2Al(OH)_6](NO_3)\cdot H_2O$ unit (spheres color code: Zn, pink; Al, light blue; O, red; N, blue; H, white) and the aluminum surfaces: = layer (electrostatic interaction), = anion (electrostatic interaction), and ⊥ normal (metal−oxygen coordination).

through the cationic layer parallel to the surface (= layer), through the interlayer contents with the cationic layer also parallel to the surface (= anion), and through the hydroxide groups of the cationic layer normal to the surface (⊥ normal).

Three models for the Al(111) slabs were used (Figure 4), all derived from a bulk aluminum structure with a lattice parameter of 4.046 Å: the first was a (4 × 4) slab with 4 layers, where the two bottom layers of the slab were kept frozen, while the other two were relaxed; the second was a (4 × 4) slab with 2 layers, where the bottom layer of the slab was kept frozen, while the other was relaxed; and the third was an (8 × 4) slab with 2 layers, where the bottom layer of the slab was kept frozen, while the other was relaxed. These three systems are labeled from now on (4 × 4)-Al(111)-4L, (4 × 4)-Al(111)-2L and (8 × 4)-Al(111)-2L, respectively. The (8 × 4)-Al(111)-2L slab model was used to study the interaction with a larger LDH−NO_3 unit, $[Zn_8Al_4(OH)_{24}](NO_3)_4\cdot 4H_2O$, whereas the (4 × 4)-Al(111)-2L slab model was used to analyze the reduction of the number of layers on the final results. For the optimization of the larger LDH−NO_3 unit, the metallic atoms of the cationic LDH layer were kept frozen in order to save computational time. This solution was also employed because in the present work, we are only interested in finding the most favorable type of interaction (with the most stable electronic energy) between the LDHs and the metallic surfaces.

The α-Al_2O_3(0001) slab consisted of an aluminum-terminated model with nine layers (Al O Al Al O Al Al O Al). The model was described as a (2 × 2) hexagonal cell, containing 12 Al_2O_3 units with a lattice parameter of a = 4.76 Å.[39] The five bottom layers were kept frozen, while the upper four were relaxed (Figure 4). The hydroxylation of the surface in the presence of water was also considered, according to the conclusions obtained by other authors.[40] The degree of hydroxylation was 75% (three hydroxyl groups per (2 × 2)

DOI: 10.1021/acs.jpcc.6b10860
J. Phys. Chem. C XXXX, XXX, XXX−XXX

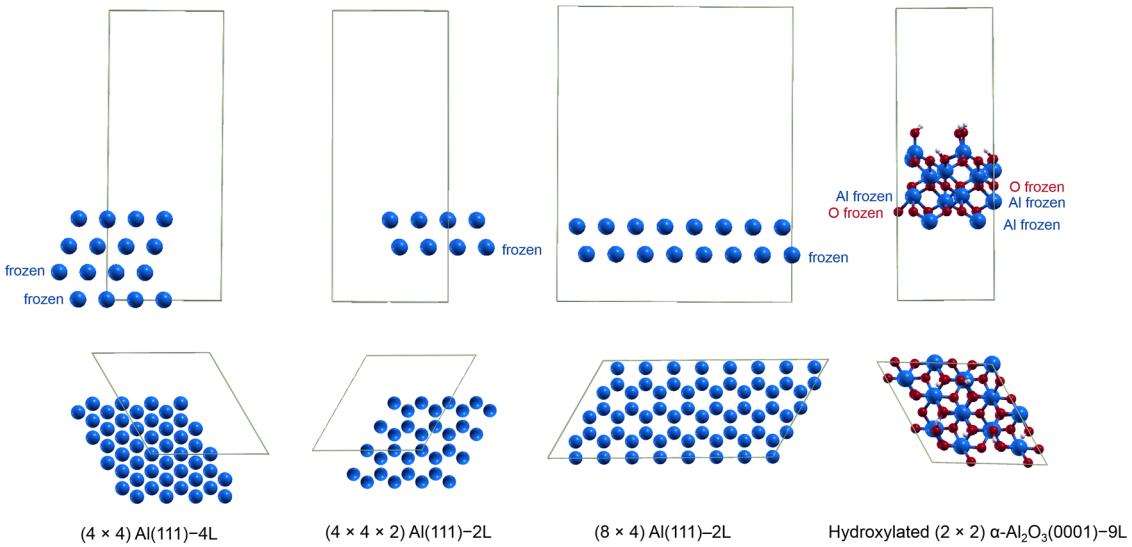

Figure 4. Representation of the supercells of (4 × 4)-Al(111)-4L, of (4 × 4)-Al(111)-2L, of (8 × 4)-Al(111)-2L, and 75%[40] hydroxylated aluminum terminated (2 × 2) α-Al_2O_3(0001)−9L model surfaces (spheres color code: Al, light blue; O, red; H, white).

supercell),[40] where each hydroxyl group binds to a surface aluminum atom and each proton binds to one of the three equivalent surface oxygens.[40]

The four systems examined in this work, (4 × 4)-Al(111)−4L·$[Zn_2Al(OH)_6](NO_3)\cdot H_2O$, (4 × 4)Al(111)−2L·$[Zn_2Al(OH)_6](NO_3)\cdot H_2O$, (8 × 4)Al(111)−2L·$[Zn_8Al_4(OH)_{24}](NO_3)_4\cdot 4H_2O$, and α-Al_2O_3(0001)−9L·$[Zn_2Al(OH)_6](NO_3)\cdot H_2O$, consisted of 86, 54, 152, and 91 atoms per supercell, respectively. In all cases, a vacuum region of at least 10 Å was kept between the top of the adsorbed molecule and the adjacent slab, and the artificial electric field perpendicular to the surface was corrected using the Bengtsson method.[41]

4. RESULTS AND DISCUSSION

Particles. Zn(2)Al−NO_3 conversion films are synthesized using similar conditions as Zn(2)Al−NO_3 particles except for the source of aluminum, which is provided from the dissolution of the aluminum alloy. For this reason, the relation between structure and morphology of LDH particles and single-layer nanosheets is first explored in this work.

To understand how crystallites constitute polycrystalline particles, four samples of LDH−NO_3, synthesized according to a previous work,[25] with different crystallite and particle sizes, were characterized by AFM (Figure 5 and Figures S1−S4 of the Supporting Information), and the plate height was measured (Table 1 and Supporting Information). The AFM results show LDH particles with typical hexagonal plate morphology. In samples (pH = 10, T = 325 K, t = 4 h) and (pH = 10, T = 373 K, t = 2 h), synthesized using lower temperatures or shorter times of hydrothermal treatment in comparison with samples (pH = 10, T = 373 K, t = 4 h) and (pH = 8.5, T = 372 K, t = 4 h), it is possible to verify much more material with smaller size and less typical morphology surrounding the LDH hexagonal plates. This is consistent with the lower crystallite and particle sizes obtained for these samples (Table 1).

According to the results presented in Table 1, the particle size is larger than the plate height. As presented in Figure 6, one possible view of the relation between structure and morphology of LDH polycrystalline particles is that a few crystallites are assembled in the direction defined by the (006) reflection

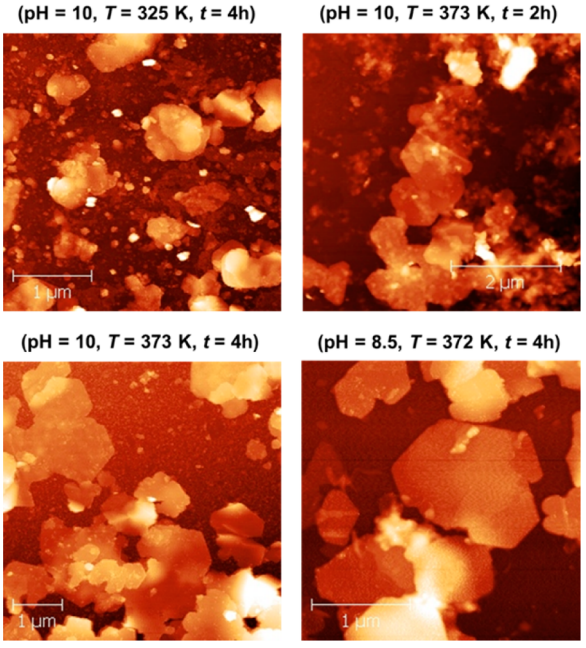

Figure 5. AFM results of LDH samples synthesized using different conditions.

Table 1. Average Crystallite Size in the Directions Perpendicular ($L_{(006)}$) and Parallel ($L_{(110)}$) to the Cationic Layers, Hydrodynamic Particle Size Defined by Its Length and the AFM Particle Plate Height, Together with Number of Particles Measured (n), for Different LDH Samples

sample	$L_{(006)}$[25]/nm	plate height (n)/nm	$L_{(110)}$[25]/nm	particle length[25]/nm
(pH = 10, T = 325 K, t = 4 h)	19 ± 2	25 ± 4 (30)	30 ± 3	341 ± 21
(pH = 10, T = 373 K, t = 2 h)	15 ± 2	44 ± 7 (16)	34 ± 2	333 ± 8
(pH = 10, T = 373 K, t = 4 h)	26 ± 2	26 ± 4 (31)	49 ± 3	400 ± 11
(pH = 8.5, T = 372 K, t = 4 h)	30 ± 2	22 ± 4 (39)	48 ± 3	445 ± 10

DOI: 10.1021/acs.jpcc.6b10860
J. Phys. Chem. C XXXX, XXX, XXX−XXX

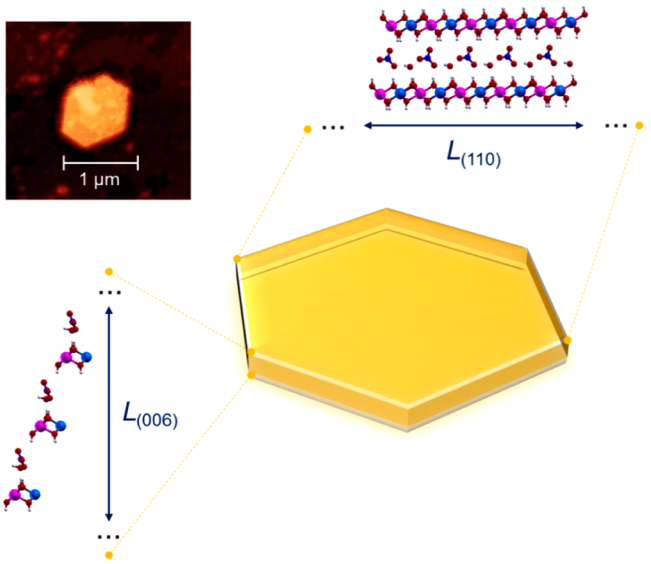

Figure 6. Example of an LDH particle obtained by AFM and molecular representation of the crystallite sizes obtained from the (006) and (110) reflections (spheres color code: Zn, pink; Al, light blue; O, red; N, blue; H, white) indicating their role in an LDH hexagonal plate.

contributing to the plate height, while a considerable number of crystallites are assembled in the direction defined by the (110) reflection resulting in the particle length.

By examining the relative surface energies presented in Figure 7, it is possible to verify that the surface energies E_x and E_y are higher than E_z, meaning that the exposed surfaces x and y are less stable than the z surface. In the light of the structure of LDH particles described earlier, these results explain why the particle length is much larger than the plate height, resulting in the alignment of cationic layers of several crystallites in the direction parallel to the well-known LDH plates (Figure 6).

Otherwise, if LDH particles were constituted by cationic layers of crystallites aligned perpendicularly to the hexagonal plates of the particles, the relative surface energy E_z should be higher than E_x and E_y (Figure 7).

Another way to look at the surface energies is that the lower stability of the surfaces resulting from interrupting the periodicity of the crystal defined by vectors x and y results in a more favorable interaction energy between the ends of these surfaces to form a fully periodic crystal (Figure 7). Consequently, considering the molecular view of the LDH plates depicted in Figure 6, this results in larger dimensions of the particles in the direction defined by the planes of the cationic layers.

In terms of chemical interactions, these results show that it is more favorable to form metal−oxygen bonds in the direction parallel to the layer than electrostatic interactions between the cationic layers and the interlayer contents (anions and water).

From the combination of surface and interaction energies with morphological results, it is demonstrated that LDH polycrystalline particles are formed, as illustrated in Figure 6, with the cationic layers aligned parallel to the observed plates defining their lateral size. The plate height resulting from the assembling of cationic layers separated by the interlayer anionic and solvent molecules is limited by the lower stability of the surface that defines this height. Therefore, it is possible to compare the values of $L(006)$ with the plate height and of $L(110)$ with the particle length (Table 1) and to determine that the particle height is defined by approximately one to three crystallites and that the particle length is defined by 8 to 11 crystallites, as represented in Figure 8. The present computational study was performed considering a 2:1 ZnAl LDH metallic ratio. Nevertheless, because of the similar nature of the interactions involved in other LDH phases (metal−oxygen bonds in the direction parallel to the cationic layers and electrostatic interactions in the direction normal to the cationic layers), our conclusions may, in principle, also be valid to other ZnAl metallic ratios, which result in particles with similar morphologies (hexagonal plates).

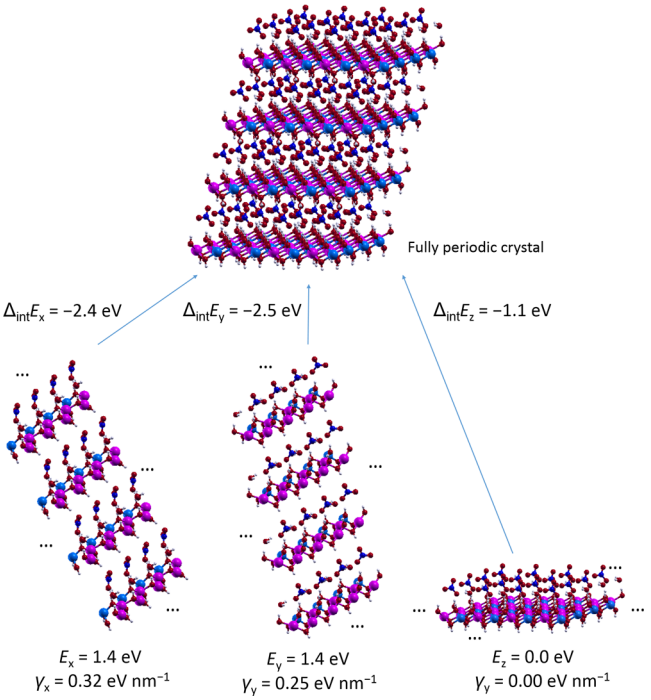

Figure 7. Relative surface energies (E_x, E_y, and E_z), relative surface energies per area (γ_x ,γ_y, and γ_z), and interaction energies ($\Delta_{int}E$) between adjacent parts of the surfaces to form a fully periodic LDH crystal (spheres color code: Zn, pink; Al, light blue; O, red; N, blue; H, white). Equations are unbalanced on purpose.

Nanosheets. The interaction energies reported in Figure 7 explain another important phenomenon involving LDHs: exfoliation. After successful exfoliation of LDH particles, several authors[18−22] have obtained plate height values of ∼0.8 nm. According to the optimized $[Zn_2Al(OH)_6](NO_3)\cdot H_2O$ supercell with a vacuum region above the surface, it is possible to conclude that the plate height is defined by approximately one brucite layer and also one layer of counterbalancing anions. The presence of the brucite layer along the nanosheets is supported by selected area electron diffraction (SAED) results[18] confirming that the (110) reflection plane is obtained after exfoliation. The nanosheets usually maintain the shapes and approximate lateral plate sizes of the original particles.[18−22] This is in agreement with the energy necessary to separate the cationic layers ($-\Delta_{int}E_z$, Figure 7), which is lower than the energy necessary to fragment them ($-\Delta_{int}E_x$ and $-\Delta_{int}E_y$, Figure 7).

The most consistent methodology to achieve the delamination of LDHs resorts to their dispersion in formamide.[18−22] Using formamide as the exfoliating agent allows LDH nanosheets to be obtained spontaneously, without the need

DOI: 10.1021/acs.jpcc.6b10860
J. Phys. Chem. C XXXX, XXX, XXX−XXX

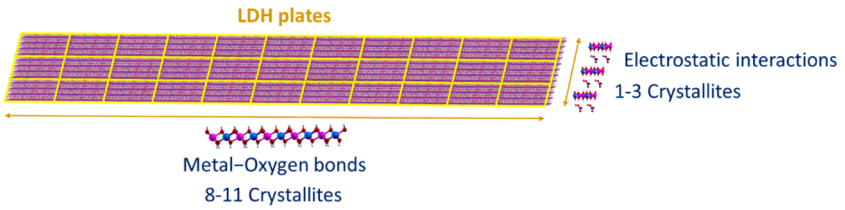

Figure 8. Number of crystallites and type of bonds responsible for the morphology of LDH particles.

of thermal treatment.[19] Nevertheless, this feature of LDHs and the role of the interlayer solvent is still not well understood.[18−22] In this work, the interlayer water molecule in Zn(2)Al−NO_3 was substituted by one formamide molecule, and the $[Zn_2Al(OH)_6](NO_3)\cdot NH_2COH$ structure was optimized.

As depicted in Figure 9, formamide holds the ability to form a network of hydrogen bonds similar to water. Each N−H in the terminal NH_2 group of formamide ($NH_2C(=O)H$) can establish a hydrogen bond with one nitrate anion as it happens with each O−H of the water molecules. Moreover, formamide can also act as a hydrogen bond acceptor through its C=O group; the latter can interact with hydrogen atoms from the hydroxyl groups of the cationic layer similarly to the oxygen atom of a water molecule. Moreover, in the case of formamide, the hydrogen atom attached to the carbonyl group can also establish C−H···O hydrogen bonds with nitrate anions while the nitrogen atom of the amino group can form N··· H−O hydrogen bonds with hydroxyl groups of the cationic layer. Therefore, the replacement of water by formamide molecules in the interlayer regions is expected to benefit from the conservation or even from the increase of the network of hydrogen bonds in the case of formamide.

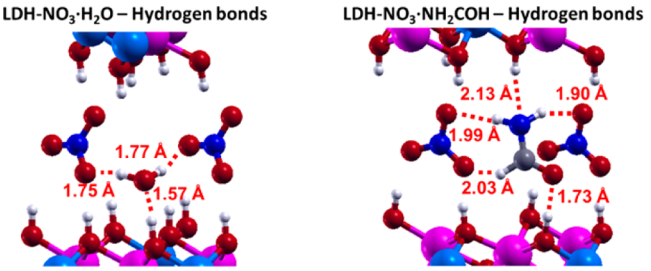

Figure 9. Hydrogen bonds and intermolecular distances for LDH−NO_3 with one water (left) and one formamide (right) molecule per anion (spheres color code: Zn, pink; Al, light blue; O, red; N, blue; H, white; C, gray).

The calculations show that the substitution of one water molecule by just one formamide molecule leads to the increase of the basal *d*-space from 9.1 to 9.5 Å (Figure 10). The basal *d*-space obtained for the solvation of the nitrate anion by one water molecule is in agreement with the experimental results.[25,38] As more solvent molecules enter the interlayer (Figure 10 and Figure S5), the increase in basal *d*-space is higher for formamide than for water. Accompanying this increase of the basal *d*-space as the number of solvent molecules per anion increase in the interlayer, there is a slight decrease of the layer separation energy for formamide and an increase for water, according to the energies obtained from DFT calculations (cf. values in Figure 10). These energetic and structural tendencies reflect the ability of formamide to delaminate LDHs in comparison to water.

The exfoliation of LDHs[18−22] can be an important process to enhance their catalytic activity[18,23] or to prepare LDHs for modification toward biocompatible drug delivery.[24] By the

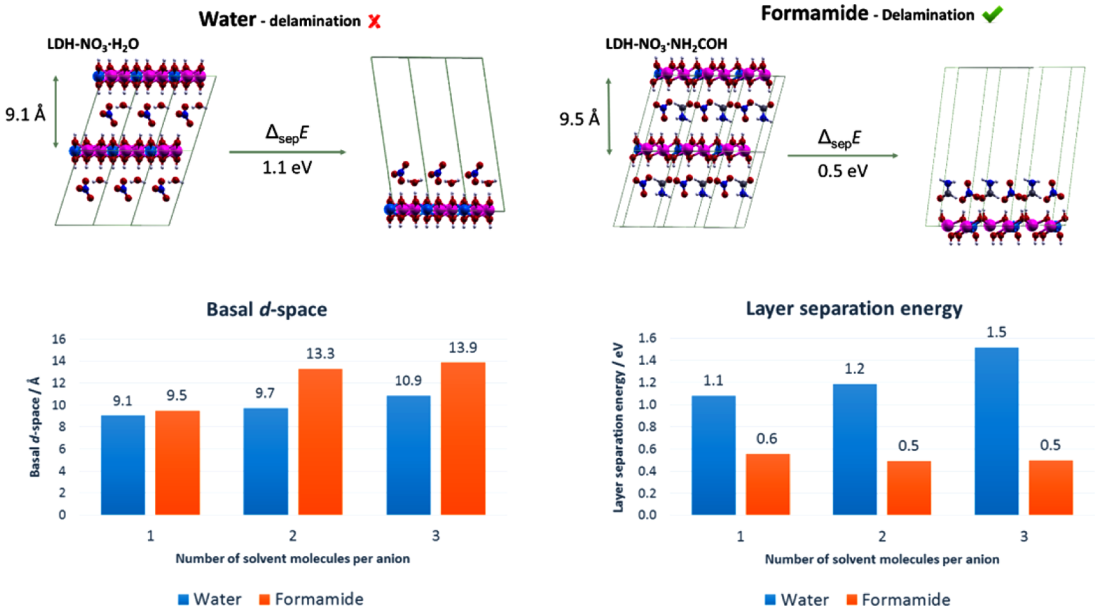

Figure 10. Basal *d*-space and layer separation energies ($\Delta_{sep}E$) for LDH−NO_3 with water and formamide as interlayer solvents (spheres color code: Zn, pink; Al, light blue; O, red; N, blue; H, white; C, gray). Equations are unbalanced on purpose.

DOI: 10.1021/acs.jpcc.6b10860
J. Phys. Chem. C XXXX, XXX, XXX−XXX

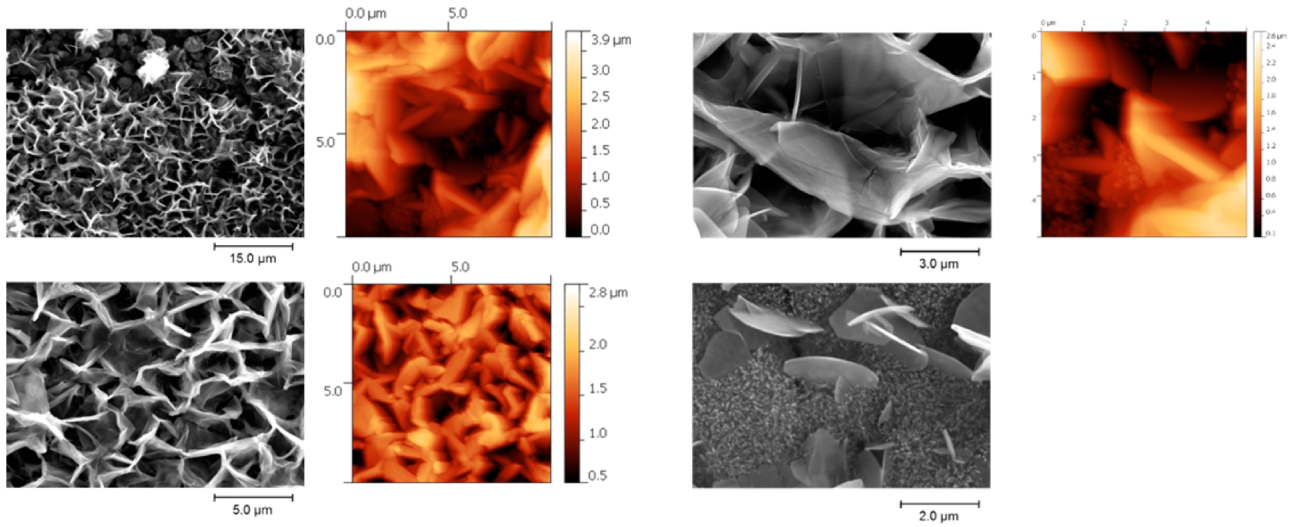

Figure 11. SEM (left) and AFM (right) images of Zn(2)Al−NO_3 conversion films on AA2024.

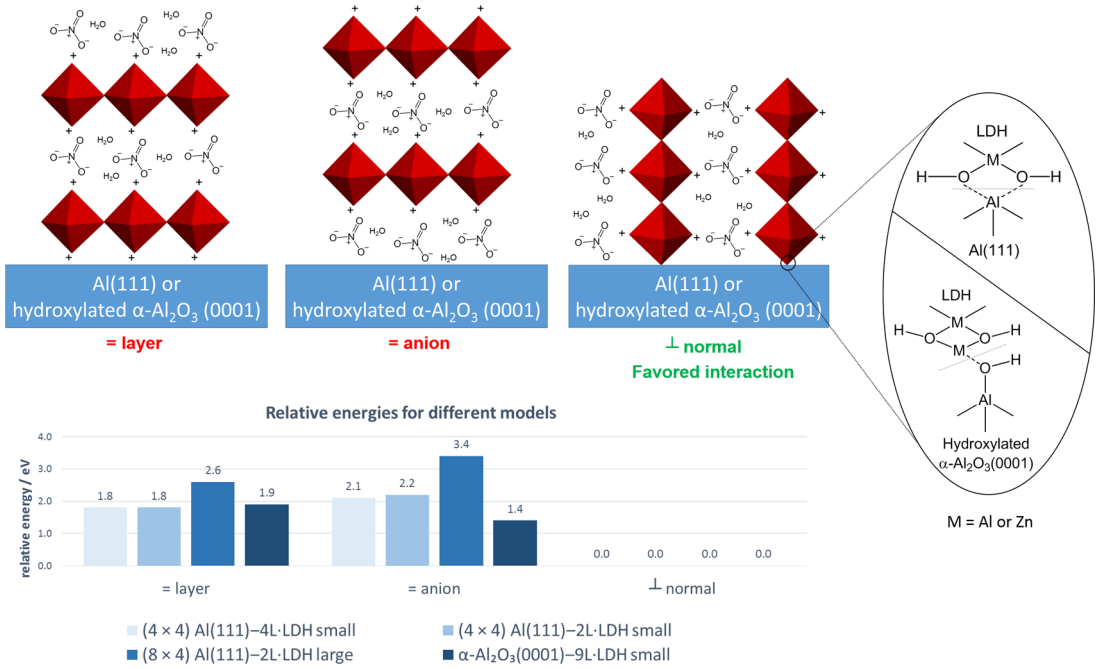

Figure 12. Results of the interaction between Zn_2Al clusters and periodic models of aluminum surfaces.

stability of the surface energies and the fact that it is the cationic layers' separation energy in the direction normal to the surface that is able to unveil the role of water and formamide in the exfoliation process, it is possible to support the role of nanosheets in defining the hexagonal plate morphology (Figure 6). Therefore, it is possible to infer about the position of the cationic layers in the morphology of conversion films.

Conversion Films. In Figure 11, it is well noticed the preference for LDH plates of conversion films to grow perpendicularly to the aluminum substrate, according to SEM and AFM images, rather than lying flat on top of the substrates and growing in height. More extensive characterization of Zn(2)Al−NO_3 conversion films grown on top of AA2024 substrates using the same methodology can be found in previous studies.[1,26,29]

Taking into account the structure of LDH plates illustrated in Figure 6 and supported by the analysis of surface energies presented in Figure 7, it is possible to conclude that LDH plates of conversion films (Figure 11) have the cationic layers perpendicular to the aluminum substrate.

The interface between Zn(2)Al−NO_3 conversion films and the aluminum surface was studied considering two extreme cases of the surface: the completely bare metal and the hydroxylated aluminum oxide. The LDH plates may interact with the aluminum oxide layer formed on top of aluminum alloys,[42] modeled by a α-Al_2O_3(0001) surface, or directly with the bare metal through defects on the oxide layer,[43] modeled by a Al(111) surface.

According to the results presented in Figure 12 and Figure S6, on both surfaces, the most favorable interaction of the LDH clusters is with the cationic layers perpendicular to the aluminum surfaces. The results are consistent across the four models examined in this study: a small $[Zn_2Al(OH)_6](NO_3)\cdot H_2O$ unit interacting with a (4 × 4)Al(111)−4L slab, a small

DOI: 10.1021/acs.jpcc.6b10860
J. Phys. Chem. C XXXX, XXX, XXX−XXX

$[Zn_2Al(OH)_6](NO_3)\cdot H_2O$ unit interacting with a (4 × 4)Al(111)−2L slab, a larger $[Zn_8Al_4(OH)_{24}](NO_3)_4\cdot 4H_2O$ unit interacting with a (8 × 4)Al(111)−2L slab, and a small $[Zn_2Al(OH)_6](NO_3)\cdot H_2O$ unit interacting with a 75% hydroxylated[40] α-Al_2O_3(0001)−9L surface. For Al(111), the hydroxyl groups of the cationic layer coordinate with the aluminum atoms of the surface. In the case of α-Al_2O_3(0001) instead, the metals of the LDH cationic layer coordinate with the hydroxyl groups resulting from the hydroxylation of the oxide surface in water.[40]

These results also elucidate the crystallization mechanism of LDH films. The mechanism has been rationalized by other authors[30,44] in terms of an initial random growth of crystal seeds. The DFT results point to a preferential orientation of seeds with the cationic layers normal to the surface even during early stages of crystal growth. After this early stage, even if seeds crystallize away from the surface in other directions, these eventually meet crystals growing with the cationic layers normal to the surface preventing the former from continuing the growing process.[30,44] The end result is the morphology observed in Figure 11.

To support the role of preferential orientation, we refer to a work relating to the growing of LDH films with different orientations on two sides of a glass substrate:[45] one bare, the other modified with poly(vinyl alcohol) (PVA). The synthetic approach used in that study also involved crystallization and hydrothermal treatment, such as the methodology employed in the conversion films analyzed herein. On the unmodified glass side, the particles were perpendicular to the surface similarly to the present study, whereas on the PVA modified glass side, the particles obtained were parallel to the surface possibly because of hydrogen bonding between the LDHs and PVA as pointed by Guo et al.[45] If there is a preferential interaction between LDH seeds and the PVA modified side,[45] it should also be true for cases where particles grow perpendicularly to the surface as shown in the present study.

The interaction between LDH clusters and metallic surfaces investigated by the present theoretical approach can be extended to other combinations of LDHs and surfaces. This approach can be used to understand the formation of LDH films in other fields beyond corrosion protection, such as OER catalysis[46] and in optical, electrical, and magnetic devices.[47]

5. CONCLUSIONS

It was shown from DFT surface energies that typical LDH particles have the cationic layers aligned parallel to the observed plate morphology defining their lateral size.

The stability of the exposed surfaces explains why LDH nanosheets obtained after exfoliation maintain approximately the same lengths and shapes of the original particles. The separation energies defined in this work together with the methodology used to comprehend the role of solvent can be useful to understand the formation of other LDH nanosheets applied in the catalysis of oxygen reduction reaction[18,23] or in biocompatible drug delivery.[24]

Combining DFT, SEM, and AFM analysis, it was established that Zn(2)Al−NO_3 conversion films formed on top of AA2024 have a preference to grow with the cationic layers perpendicular to the surface. The interface between the particles and the metallic surfaces was investigated by adsorbing Zn(2)Al−NO_3 clusters onto Al(111) and hydroxylated α-Al_2O_3(0001) surfaces. It was verified for both surfaces that the most favorable interaction is with the cationic layer perpendicular to the surface, thus explaining the morphology of the conversion films and their crystallization process. The models used herein can be adapted to other LDH systems with different metals and anions, as well as to other metallic surfaces, and to describe systems used in corrosion protection,[1] OER catalysis,[46] and in optical, electrical, and magnetic devices.[47]

■ ASSOCIATED CONTENT

Supporting Information

The Supporting Information is available free of charge on the ACS Publications website at DOI: 10.1021/acs.jpcc.6b10860.

AFM images, DFT energies, and Cartesian coordinates (PDF)

■ AUTHOR INFORMATION

Corresponding Authors

*E-mail: tlpgalvao@ua.pt. Phone: +351938403485.

*E-mail: joao.tedim@ua.pt. Phone: +351961688838.

ORCID

Tiago L. P. Galvão: 0000-0002-0685-3675

José R. B. Gomes: 0000-0001-5993-1385

Notes

The authors declare no competing financial interest.

■ ACKNOWLEDGMENTS

This work was developed in the scope of the project CICECO − Aveiro Institute of Materials, POCI-01-0145-FEDER-007679 (ref. FCT UID/CTM/50011/2013), financed by national funds through the FCT/MEC and when applicable cofinanced by FEDER under the PT2020 Partnership Agreement. Financed in the framework of project reference PTDC/QEQ-QFI/4719/2014, funded by Project 3599 - Promover a Produção Científica e Desenvolvimento Tecnológico e a Constituição de Redes Temáticas (3599-PPCDT) and FEDER funds through COMPETE 2020, Programa Operacional Competitividade e Internacionalização (POCI). The authors also thank financial support from FCT and COMPETE (PTDC/CTM-MAT/1515/2012 and Programa Investigador FCT). J.T. thanks FCT for the research grant IF/00347/2013. This work has received funding from the European Union's Horizon 2020 research and innovation programme under the Marie Skłodowska-Curie grant agreements No 645662 and No 645676. This work has also received funding from the European Union's Seventh Framework Programme (FP7/2012-2016) under the grant agreement no. 280759.

■ REFERENCES

(1) Tedim, J.; Zheludkevich, M. L.; Salak, A. N.; Lisenkov, A.; Ferreira, M. G. S. Nanostructured LDH-Container Layer with Active Protection Functionality. *J. Mater. Chem.* **2011**, *21*, 15464−15470.

(2) Liu, K.; Xu, Y.; Yao, Z.; Miras, H. N.; Song, Y.-F. Polyoxometalate-Intercalated Layered Double Hydroxides as Efficient and Recyclable Bifunctional Catalysts for Cascade Reactions. *ChemCatChem* **2016**, *8*, 929−937.

(3) Zhang, J.; Hu, H.; Li, Z.; Lou, X. W. D. Double-Shelled Nanocages with Cobalt Hydroxide Inner Shell and Layered Double Hydroxides Outer Shell as High-Efficiency Polysulfide Mediator for Lithium-Sulfur Batteries. *Angew. Chem., Int. Ed.* **2016**, *55*, 3982−3986.

(4) Sajid, M.; Basheer, C. Layered Double Hydroxides: Emerging Sorbent Materials for Analytical Extractions. *TrAC, Trends Anal. Chem.* **2016**, *75*, 174−182.

(5) Rocha, M. A.; Petersen, P. A. D.; Teixeira-Neto, E.; Petrilli, H. M.; Leroux, F.; Taviot-Gueho, C.; Constantino, V. R. L. Layered

DOI: 10.1021/acs.jpcc.6b10860
J. Phys. Chem. C XXXX, XXX, XXX−XXX

Double Hydroxide and Sulindac Coiled and Scrolled Nanoassemblies for Storage and Drug Release. *RSC Adv.* **2016**, *6*, 16419−16436.
(6) Zheludkevich, M. L.; Tedim, J.; Ferreira, M. G. S. "Smart" coatings for Active Corrosion Protection Based on Multi-Functional Micro and Nanocontainers. *Electrochim. Acta* **2012**, *82*, 314−323.
(7) Tedim, J.; Poznyak, S. K.; Kuznetsova, A.; Raps, D.; Hack, T.; Zheludkevich, M. L.; Ferreira, M. G. S. Enhancement of Active Corrosion Protection via Combination of Inhibitor-Loaded Nanocontainers. *ACS Appl. Mater. Interfaces* **2010**, *2*, 1528−1535.
(8) Tedim, J.; Kuznetsova, A.; Salak, A. N.; Montemor, F.; Snihirova, D.; Pilz, M.; Zheludkevich, M. L.; Ferreira, M. G. S. Zn-Al Layered Double Hydroxides as Chloride Nanotraps in Active Protective Coatings. *Corros. Sci.* **2012**, *55*, 1−4.
(9) Chang, Z.; Wu, C.; Song, S.; Kuang, Y.; Lei, X.; Wang, L.; Sun, X. Synthesis Mechanism Study of Layered Double Hydroxides Based on Nanoseparation. *Inorg. Chem.* **2013**, *52*, 8694−8698.
(10) Paikaray, S.; Gomez, M. A.; Jim Hendry, M.; Essilfie-Dughan, J. Formation Mechanism of Layered Double Hydroxides in Mg^{2+}-, Al^{3+}-, and Fe^{3+}-Rich Aqueous Media: Implications for Neutralization in Acid Leach Ore Milling. *Appl. Clay Sci.* **2014**, *101*, 579−590.
(11) Sun, X.; Neuperger, E.; Dey, S. K. Insights into the Synthesis of Layered Double Hydroxide (LDH) Nanoparticles: Part 1. Optimization and Controlled Synthesis of Chloride-Intercalated LDH. *J. Colloid Interface Sci.* **2015**, *459*, 264−272.
(12) Sun, X.; Dey, S. K. Insights into the Synthesis of Layered Double Hydroxide (LDH) Nanoparticles: Part 2. Formation Mechanisms of LDH. *J. Colloid Interface Sci.* **2015**, *458*, 160−168.
(13) Pushparaj, S. S. C.; Forano, C.; Prevot, V.; Lipton, A. S.; Rees, G. J.; Hanna, J. V.; Nielsen, U. G. How the Method of Synthesis Governs the Local and Global Structure of Zinc Aluminum Layered Double Hydroxides. *J. Phys. Chem. C* **2015**, *119*, 27695−27707.
(14) Tokudome, Y.; Morimoto, T.; Tarutani, N.; Vaz, P. D.; Nunes, C. D.; Prevot, V.; Stenning, G. B. G.; Takahashi, M. Layered Double Hydroxide Nanoclusters: Aqueous, Concentrated, Stable, and Catalytically Active Colloids toward Green Chemistry. *ACS Nano* **2016**, *10*, 5550−5559.
(15) Lv, W.; Du, M.; Ye, W.; Zheng, Q. The Formation Mechanism of Layered Double Hydroxide Nanoscrolls by Facile Trinal-Phase Hydrothermal Treatment and Their Adsorption Properties. *J. Mater. Chem. A* **2015**, *3*, 23395−23402.
(16) Li, W.; Livi, K. J. T.; Xu, W.; Siebecker, M. G.; Wang, Y.; Phillips, B. L.; Sparks, D. L. Formation of Crystalline Zn-Al Layered Double Hydroxide Precipitates on γ-Alumina: The Role of Mineral Dissolution. *Environ. Sci. Technol.* **2012**, *46*, 11670−11677.
(17) Stimpfling, T.; Langry, A.; Hintze-Bruening, H.; Leroux, F. In Situ Platelets Formation into Aqueous Polymer Colloids: The Topochemical Transformation from Single to Double Layered Hydroxide (LSH-LDH) Uncovered. *J. Colloid Interface Sci.* **2016**, *462*, 260−271.
(18) Song, F.; Hu, X. Exfoliation of Layered Double Hydroxides for Enhanced Oxygen Evolution Catalysis. *Nat. Commun.* **2014**, *5*, 4477.
(19) Ma, R.; Liu, Z.; Li, L.; Iyi, N.; Sasaki, T. Exfoliating Layered Double Hydroxides in Formamide: A Method to Obtain Positively Charged Nanosheets. *J. Mater. Chem.* **2006**, *16*, 3809−3813.
(20) Liu, Z.; Ma, R.; Osada, M.; Iyi, N.; Ebina, Y.; Takada, K.; Sasaki, T. Synthesis, Anion Exchange, and Delamination of Co-Al Layered Double Hydroxide: Assembly of the Exfoliated Nanosheet/polyanion Composite Films and Magneto-Optical Studies. *J. Am. Chem. Soc.* **2006**, *128*, 4872−4880.
(21) Han, J. Bin; Lu, J.; Wei, M.; Wang, Z. L.; Duan, X. Heterogeneous Ultrathin Films Fabricated by Alternate Assembly of Exfoliated Layered Double Hydroxides and Polyanion. *Chem. Commun.* **2008**, *41*, 5188−5190.
(22) Abellán, G.; Coronado, E.; Martí-Gastaldo, C.; Pinilla-Cienfuegos, E.; Ribera, A. Hexagonal Nanosheets from the Exfoliation of Ni^{2+}-Fe^{3+} LDHs: A Route towards Layered Multifunctional Materials. *J. Mater. Chem.* **2010**, *20*, 7451−7455.
(23) Liang, H.; Meng, F.; Cabán-Acevedo, M.; Li, L.; Forticaux, A.; Xiu, L.; Wang, Z.; Jin, S. Hydrothermal Continuous Flow Synthesis and Exfoliation of NiCo Layered Double Hydroxide Nanosheets for Enhanced Oxygen Evolution Catalysis. *Nano Lett.* **2015**, *15*, 1421−1427.
(24) Nicolosi, V.; Chhowalla, M.; Kanatzidis, M. G.; Strano, M. S.; Coleman, J. N. Liquid Exfoliation of Layered Materials. *Science (Washington, DC, U. S.)* **2013**, *340*, 1226419.
(25) Galvão, T. L. P.; Neves, C. S.; Caetano, A. P. F.; Maia, F.; Mata, D.; Malheiro, E.; Ferreira, M. J.; Bastos, A. C.; Salak, A. N.; Gomes, J. R. B.; et al. Control of Crystallite and Particle Size in the Synthesis of Layered Double Hydroxides: Macromolecular Insights and a Complementary Modeling Tool. *J. Colloid Interface Sci.* **2016**, *468*, 86−94.
(26) Tedim, J.; Zheludkevich, M. L.; Bastos, A. C.; Salak, A. N.; Carneiro, J.; Maia, F.; Lisenkov, A. D.; Oliveira, A. B.; Ferreira, M. G. S. Effect of Surface Treatment on the Performance of LDH Conversion Films. *ECS Electrochem. Lett.* **2014**, *3*, C4−C8.
(27) Twite, R. L.; Bierwagen, G. P. Review of Alternatives to Chromate for Corrosion Protection of Aluminum Aerospace Alloys. *Prog. Org. Coat.* **1998**, *33*, 91−100.
(28) Tedim, J.; Bastos, A. C.; Kallip, S.; Zheludkevich, M. L.; Ferreira, M. G. S. Corrosion Protection of AA2024-T3 by LDH Conversion Films. Analysis of SVET Results. *Electrochim. Acta* **2016**, *210*, 215−224.
(29) Tedim, J.; Zheludkevich, M. L.; Bastos, A. C.; Salak, A. N.; Lisenkov, A. D.; Ferreira, M. G. S. Influence of Preparation Conditions of Layered Double Hydroxide Conversion Films on Corrosion Protection. *Electrochim. Acta* **2014**, *117*, 164−171.
(30) Guo, X.; Xu, S.; Zhao, L.; Lu, W.; Zhang, F.; Evans, D. G.; Duan, X. One-Step Hydrothermal Crystallization of a Layered Double Hydroxide/alumina Bilayer Film on Aluminum and Its Corrosion Resistance Properties. *Langmuir* **2009**, *25*, 9894−9897.
(31) Giannozzi, P.; Baroni, S.; Bonini, N.; Calandra, M.; Car, R.; Cavazzoni, C.; Ceresoli, D.; Chiarotti, G. L.; Cococcioni, M.; Dabo, I.; et al. QUANTUM ESPRESSO: A Modular and Open-Source Software Project for Quantum Simulations of Materials. *J. Phys.: Condens. Matter* **2009**, *21*, 395502.
(32) Perdew, J. P.; Burke, K.; Ernzerhof, M. Generalized Gradient Approximation Made Simple. *Phys. Rev. Lett.* **1996**, *77*, 3865−3868.
(33) Costa, D. G.; Rocha, A. B.; Diniz, R.; Souza, W. F.; Chiaro, S. S. X.; Leitão, A. A. Structural Model Proposition and Thermodynamic and Vibrational Analysis of Hydrotalcite-Like Compounds by DFT Calculations. *J. Phys. Chem. C* **2010**, *114*, 14133−14140.
(34) Vanderbilt, D. Soft Self-Consistent Pseudopotentials in a Generalized Eigenvalue Formalism. *Phys. Rev. B: Condens. Matter Mater. Phys.* **1990**, *41*, 7892−7895.
(35) Marzari, N.; Vanderbilt, D.; De Vita, A.; Payne, M. C. Thermal Contraction and Disordering of the Al(110) Surface. *Phys. Rev. Lett.* **1999**, *82*, 3296−3299.
(36) Monkhorst, H. J.; Pack, J. D. Special Points for Brillouin-Zone Integrations. *Phys. Rev. B* **1976**, *13*, 5188−5192.
(37) Costa, D. G.; Rocha, A. B.; Souza, W. F.; Chiaro, S. S. X.; Leitão, A. Comparative Structural, Thermodynamic and Electronic Analyses of $Zn^{-}Al^{-}A^{n-}$ Hydrotalcite-like Compounds (A^{n-} = Cl^{-}, F^{-}, Br^{-}, OH^{-}, CO_3^{2-} or NO_3^{-}): An Ab Initio Study. *Appl. Clay Sci.* **2012**, *56*, 16−22.
(38) Carneiro, J.; Caetano, A. F.; Kuznetsova, A.; Maia, F.; Salak, A. N.; Tedim, J.; Scharnagl, N.; Zheludkevich, M. L.; Ferreira, M. G. S. Polyelectrolyte-Modified Layered Double Hydroxide Nanocontainers as Vehicles for Combined Inhibitors. *RSC Adv.* **2015**, *5*, 39916−39929.
(39) Schreyer, M.; Guo, L.; Thirunahari, S.; Gao, F.; Garland, M. Simultaneous Determination of Several Crystal Structures from Powder Mixtures: The Combination of Powder X-Ray Diffraction, Band-Target Entropy Minimization and Rietveld Methods. *J. Appl. Crystallogr.* **2014**, *47*, 659−667.
(40) Rohmann, C.; Metson, J. B.; Idriss, H. A DFT Study on Carbon Monoxide Adsorption onto Hydroxylated α-Al_2O_3(0001) Surfaces. *Phys. Chem. Chem. Phys.* **2014**, *16*, 14287−14297.

DOI: 10.1021/acs.jpcc.6b10860
J. Phys. Chem. C XXXX, XXX, XXX−XXX

694 (41) Bengtsson, L. Dipole Correction for Surface Supercell
695 Calculations. *Phys. Rev. B: Condens. Matter Mater. Phys.* **1999**, *59*,
696 12301−12304.
697 (42) Campbell, T.; Kalia, R. K.; Nakano, A.; Vashishta, P.; Ogata, S.;
698 Rodgers, S. Dynamics of Oxidation of Aluminum Nanoclusters Using
699 Variable Charge Molecular-Dynamics Simulations on Parallel Com-
700 puters. *Phys. Rev. Lett.* **1999**, *82*, 4866−4869.
701 (43) Thompson, G. E.; Shimizu, K.; Wood, G. C. Observation of
702 Flaws in Anodic Films on Aluminium. *Nature* **1980**, *286*, 471−472.
703 (44) Lee, W.; Kim, E.; Choi, J.; Lee, K. B. Kinetic Analysis of
704 Secondary Crystal Growth for Hydrotalcite Film Formation. *Cryst.*
705 *Growth Des.* **2015**, *15*, 884−890.
706 (45) Guo, X.; Zhang, F.; Xu, S.; Evans, D. G.; Duan, X. Preparation
707 of Layered Double Hydroxide Films with Different Orientations on
708 the Opposite Sides of a Glass Substrate by in Situ Hydrothermal
709 Crystallization. *Chem. Commun.* **2009**, *44*, 6836−6838.
710 (46) Lu, Z.; Xu, W.; Zhu, W.; Yang, Q.; Lei, X.; Liu, J.; Li, Y.; Sun, X.;
711 Duan, X. Three-Dimensional NiFe Layered Double Hydroxide Film
712 for High-Efficiency Oxygen Evolution Reaction. *Chem. Commun.* **2014**,
713 *50*, 6479−6482.
714 (47) Guo, X.; Zhang, F.; Evans, D. G.; Duan, X. Layered Double
715 Hydroxide Films: Synthesis, Properties and Applications. *Chem.*
716 *Commun.* **2010**, *46*, 5197−5210.

DOI: 10.1021/acs.jpcc.6b10860
J. Phys. Chem. C XXXX, XXX, XXX−XXX